Hydraulic tunnels with shotcrete linings

Ana Silva Tavares[1]

September, 2014

[1] M.Sc. Student, Instituto Superior Técnico, Av. Rovisco Pais, 1, 1049-001 Lisboa, Portugal; *anasilvatavares14@gmail.com*

ABSTRACT: Due to safety, functionality and durability criteria, hydraulic tunnels are usually designed with reinforced concrete solutions. Over the past years, this traditional lining system has been replaced by shotcrete designed solutions, that are often more economical and have greater simplicity of application.

The intent of the present work is to analyse the feasibility of the new solutions by studying the case of the outlet tunnel of hydraulic circuit of Salamonde dam. In order to achieve that, it was performed a bibliographic survey about the response of a rock mass to the tunnelling and the different design and solution alternatives. All results of geological investigation, geotechnical characterization and devised cartographies during the advance of the excavation face were also analysed. Using numerical calculation software, and combining it with the collected information, a stress-strain and seepage numerical analysis of some constructive solutions was carried out.

This study aimed at validating the obtained results by comparing them with the ones monitored *in situ* and to ensure that they meet the safety requirements. Thus it was possible to verify the adequacy of the adopted solutions and to suggest new ones.

After presenting the set of new solutions, some suggestions for future developments are also presented.

KEYWORDS: hydraulic tunnel; rock mass classifications; tunnel linings, reinforced shotcrete; numerical modelling.

1 INTRODUCTION

In the last few years EDP decided to make some power reinforcement works in dams. It is in one of this works that the “Salamonde II” project fits in. Contrary to road tunnels, hydraulic tunnels have the particularity of being in permanent solicitation, caused by the water flow, which results in stronger design requirements.

However, it has been proven that for hydraulic tunnels with low pressure and free surface that there is no need for such solutions. If the rock mass has good quality, a simple shotcrete solution with punctual ground nails in loose blocks will be enough to sustain the stress relief.

Even though this is seemed to be the ideal solution, the lack of case studies and experience, may result in oversized designs due to safety reasons.

The purpose of this work is then, after studying all the local geological and geotechnical information, to analyse the behaviour of the three different situations (no support, fibber reinforced shotcrete lining and reinforced concrete lining) in the tunnel cross sections that are believed to be less stable. That analysis is developed with the help of 2D and 3D numerical modelling software (Plaxis).

As a result, it will be presented the best solution for each tunnel cross section in study, according to the rock mass quality and hydrogeological conditions.

2 ROCK MECHANICS

There is a main difference between soil and rock mechanics when it comes to solve stability problems. In the first case, the mass is treated as a continuous material, meaning that the failure occurs on the soil mass itself, while in rock mechanics the failure occurs through the rock mass’ discontinuities.

Discontinuities include a range of sizes and forms such as joints, lamination planes, foliation planes, lithological contact surfaces and faults (Vallejo and Ferrer, 2011). They can be characterized by six features: orientation, defined by its dip and dip direction; spacing, the average distance between discontinuity planes in the same set; continuity, meaning the area of the discontinuity; fill; roughness and aperture, i.e., the distance separating the discontinuity walls when there is no fill (Vallejo and Ferrer, 2011).

Failure of rock masses in tunnel works are very common and they occur due to the unfavourable intersection of joints or faults by the tunnel excavation. represents three possible causes of instability: complete shear failure (a), buckling failure (b) and tensile splitting shearing and sliding (c) (Aydan *et al*., 1993).

ROCK MASS CLASSIFICATIONS

In order to characterize rock masses, classification systems have been developed over the last decades to allow

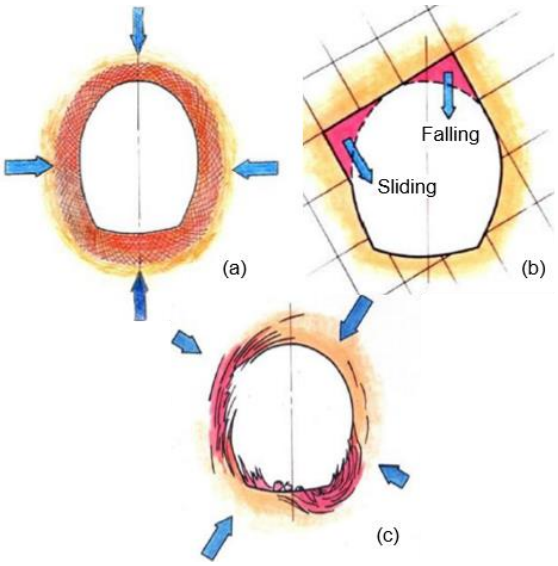

Fig. 1 – Classification of failure forms of tunnel in squeezing rocks (Hoek, 2008 apud Álvarez, 2012)

engineers to group this materials according to their suitability for different uses, being the most important ones the Rock Mass Rating (RMR) (Bienawski, 1983), the Q index (Barton *et al*., 1974) and the Geological Strength Index (GSI) (Hoek, 1994) classifications.

Table 1 indicates the five different classes of RMR according to the rock mass quality.

Table 1 – Rock mass classes (Bienawski, 1989)

Class	**I**	**II**	**III**	**IV**	**V**
Description	Very Good	Good	Fair	Poor	Very Poor
Rating	100-81	80-61	60-41	40-21	<20

The **GSI** evaluates a rock mass quality based on the extent of the degree and characteristics of fracturing, geological structure, block size and discontinuity weathering. Unlike the other indexes, this one is based only on visual analysis.

MOHR-COULOMB AND HOEK-BROWN CRITERIA

The **Mohr-Coulomb** (M-C) failure criterion can exclusively be applied to continuum masses, but due to its simplicity and flexibility it is often used in rock engineering modelling and design. The constitutive elasto-plastic model associated to this criterion uses the elastic properties expressed by E (Young modulus), υ (Poisson ratio), and the following strength parameters, ϕ'(friction angle in terms of effective stresses), c' (apparent cohesion) and ψ (dilatancy angle).

The **Hoek and Brown** (H-B) criteria is originally an empirical method applied to intact rocks or isotropic rocks in which the existent discontinuities are so close that ground can be assumed to have a continuum behaviour. But if associated to the GSI it is possible to obtain a generalized Hoek-Brown Criterion (Hoek *et al*., 2002), applied to rock masses, expressed as:

$$\sigma_1{}' = \sigma_3{}' + \sigma'_{ci}\left(m_b\frac{\sigma_3{}'}{\sigma_{ci}} + s\right)^a \qquad (1)$$

where $\sigma_1{}'$ and $\sigma_3{}'$ are the major and minor principal stresses, m_b is a reduced value of the intact material constant m_i, s and a are constants for the rock mass.

The H-B criterion is probably the most appropriate when it comes to rock mass analysis. Nevertheless, the majority of current geotechnical software still uses M-C formulation. Therefore, it is necessary to determine equivalent values of ϕ' and c'. This process comes from the adjustment of the non-linear relation between σ_1' and $\sigma_3{}'$ (H-B) to the linear one (M-C), in the range of the applied stresses (Fig. 2). The interaction between the two equations represented in Fig. 2, results in:

$$\phi' = \sin^{-1}\left[\frac{6am_b(s+m_b\sigma'_{3n})^{a-1}}{2(1+a)(2+a)+6am_b(s+m_b\sigma'_{3n})^{a-1}}\right] \qquad (2)$$

$$c' = \frac{\sigma_{ci}[(1+2a)s+(1-a)m_b\sigma'_{3n}](s+m_b\sigma'_{3n})^{a-1}}{(1+a)(2+a)\sqrt{1+\frac{6am_b(s+m_b\sigma'_{3n})^{a-1}}{(1+a)(2+a)}}} \qquad (3)$$

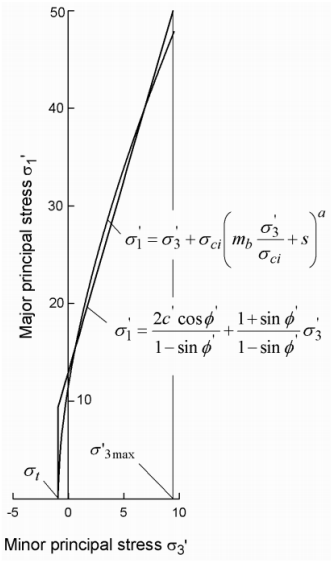

Fig. 2 - Relationship between major and minor principal stresses for Hoek-Brown and equivalent Mohr-Coulomb criteria (Hoek et al., 2002)

STRESS AND STRAIN IN ROCK MASSES

To define the elastic behaviour of an isotropic rock it is only necessary two of the following five constants: E, Young's Modulus; υ, Poisson's coeficient; λ, Lamé's coefficient; G, shear modulus and K, the bulk modulus. All the last five constants are related, but E and υ are usually the most used in engineering problems.

The intact rock elastic response does not directly indicates the way a rock mass will behave, but it is still very important as a quality index.

So, in order to obtain the necessary strength and deformation parameters to perform ulterior construction decisions, it is necessary to make some laboratory tests in intact rock samples (point-load test, triaxial test, sound wave velocity test, among others) and also *in situ* tests to measure the actual *in situ* stresses and strength.

In Situ Tests

The four test recommended by the International Society for Rock Mechanics (Kim and Franklin, 1987) are the flatjack test, hydraulic fracturing technique, USBM – type drill hole deformation gauge and CSIRO – type cell with 9 or 12 strain gauges. Table 2 shows the stress components that can be determined by each method. Due to its current use the STT (Stress Tensor Tube) test is also very common.

The STT test is the only one of mentioned that was performed in the Salamonde's outlet tunnel. This *in situ* test consists in measuring the released stresses by 3D strain gauges while the measurement zone is overcored. The resulting core can be later used for triaxial tests, in order to determine the strength parameters. Fig. 3 shows the main steps of this test.

Table 2 – Stress components supplied by different measurement methods (Hudson and Harrison, 1997)

Flatjack test	$\begin{bmatrix} \sigma_{xx} & \tau_{xy} & \tau_{xz} \\ & \sigma_{yy} & \tau_{yz} \\ & & \sigma_{zz} \end{bmatrix}$		Only one normal stress component determined
Hydraulic fracturing	$\begin{bmatrix} \sigma_1 & 0 & 0 \\ & \sigma_2 & 0 \\ & & \sigma_3 \end{bmatrix}$		Principal stresses assumed parallel to axes
Overcoring Tests	**USBM**	$\begin{bmatrix} \sigma_{xx} & \tau_{xy} & \tau_{xz} \\ & \sigma_{yy} & \tau_{yz} \\ & & \sigma_{zz} \end{bmatrix}$	Three components in 2D determined from 3 measurements
	CSIRO &STT	$\begin{bmatrix} \sigma_{xx} & \tau_{xy} & \tau_{xz} \\ & \sigma_{yy} & \tau_{yz} \\ & & \sigma_{zz} \end{bmatrix}$	All six components determined from six measurements of strain at one time

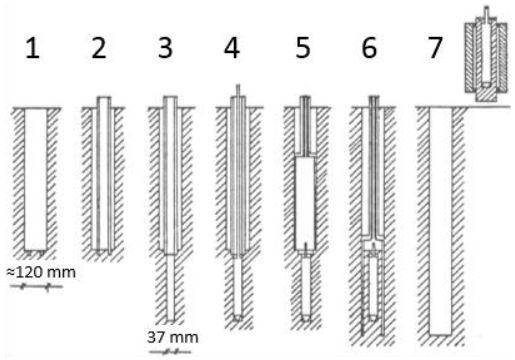

Fig. 3 - STT test technique (Lamas and Figueiredo, 2009)

Strength Parameters Correlations with Empiric Methods

This method has been under researchers radars during recent decades due to its widespread application and lack of tests and costs. It can be obtain by using a representative value of a rock mass index, i.e., RMR, Q or GSI. As a simplistic method, it is very important to use the result with some caution and a conservative eye, due to the uncertainty level. Table 3 shows some known correlations between the Young's modulus, *E*, and some rock masses quality indexes.

Table 3 – Correlations for Young's modulus, E

Authors	Application	Equation
Bieniawski, 1978	Good rock mass quality: RMR>50-55	$E = 2RMR - 100$ (GPa)
Serafim e Pereira, 1983	Fair to bad rock mass quality: 10<RMR<50 and 1<E<10 GPa	$E = 10^{(RMR-10)/40}$ (GPa)
Barton, 1995, 2006	Jointed and faulted rock mass	$E = 10Q_c{}^{1/3}$(GPa); $Qc = Q.\sigma_{ci}/100$ (σ_{ci} em MPa)
Hoek & Dieiderichs, 2006	20<GSI<80 D=0 (non distributed rock mass) D=1 (distributed rock mass)	$E = 100{,}000\left(\frac{1-D/2}{1+e^{(75+25D-GSI)/11}}\right)$ (MPa)

3 Tunnels

Underground works and tunnels are the perfect solution to overcome issues as high urban density or mountainous areas. Tunnels are not only a way to increase the road and rail pathways but they can also be used for hydraulic, energy or electric purposes.

The first step in a tunnel design is to perform, as mentioned before, the necessary geologic and geotechnical investigations in order to predict the zoning of the surrounding ground of the tunnel. Knowing the purpose of tunnel, it is then possible to design the primary support and the permanent lining, where the former has a structural function only until the latter is built.

Rock Mass Tunnel Design

Currently, it is very common to use **empirical methods** to define the type of support to be used. These methods are based on rock masses quality index, such as *RMR*, *Q* and *GSI*.

Through the RMR index it is possible to estimate the time that, according with spam length, the rock mass will be stable without any kind of support. Fig. 4 shows an abacus that relates all these variables.

Another way to design and predict the tunnel response is by using **numerical analysis**, i.e., computer software that use the Finite Element Method (FEM), the Finite Difference Method (FDM), Boundary Elements Method (BEM) or Discrete Element Method (DEM).

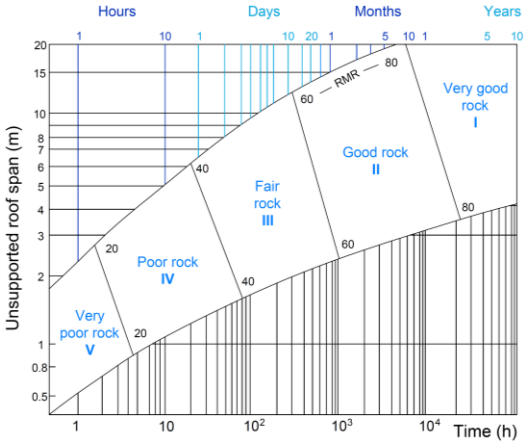

Fig. 4 – Unsupported roof span and stand-up time for various rock mass classes according with RMR (Bienawski, 1989)

The finite element programs used in this work are the Plaxis 3D tunnel and Plaxis 2D, which simulates the ground by dividing the domain in similar triangular finite elements with the homogenous individual characteristics.

Plaxis 3D tunnel simulates volume by repeating the same 2D model lengthwise, dividing the domain in slices.

Shotcrete Lining

This support solution has come to replace the conventional ones (reinforced concrete), over the last years. Its main advantages are (Vandewalle, 2005):

- enhance the compactness and strength of the rock mass, by filling joints and faults (high adhesion);
- hydrates and oxidates the rock, which results in deterioration prevention;
- rapid hardening;
- redirect and contains the water flow;
- fast and economic method;
- flexibility in the cross-section shape form and dimensions.

Despite all this, shotcrete, by itself, is still useless when it comes to resist tensile stresses, as any other concrete. In order to resolve this issue, steel fibbers can be introduced in the wet mix, enhancing ductility, strength, impacts and the energy absorption (SFRS). There are many types of fibers and they all allow to form a very homogeneous slurry, which also improves the lining fire resistance.

Elastic Design

Shotcrete design can be done assuming elastic behaviour and verified by the expression:

$$f_{adm} \geq \frac{N}{e} \pm \frac{M}{w} \qquad (4)$$

where f_{adm} is the elastic admissible stress of the SFRS, assumed to be 13 MPa (deducted from Vandewalle, 2005), M is the bending moment per unit length, N is the axial load per unit length, e is the section thickness and w is the bending modulus ($w = \frac{e^2}{6}$).

4 Salamonde's Outlet Tunnel

The tunnel in analysed is part of the Salamonde's dam power reinforcement EDP project. The works started in 2010 and will be concluded in middle 2015. The tunnel has a length of 2,2 km that crosses areas with 400 meters cover (Fig. 8).

The geotechnical investigation includes 15 boreholes. The main tests performed include:

- STT in situ tests;
- Lugeon permeability tests;
- uniaxial compressive strength;
- density tests;
- triaxial shear tests.

Based on the test results, the designers defined four different geotechnical zones, and associated each zone to a standard design solution.

Zone	Weathering (W)	Fracturing (F)	GSI	RMR	Class
ZG1	≤W2	≤F2	70-85	>70	II a I

Solution A: 5 cm of SFRS; 5 cm of simple shotcrete; A500 nails with A_{inf} (influence area)=4.50 m^2; L=4.00 m ; ϕ25 mm.

ZG2	W2 a W3	F2 a F3	50-70	50-70	III a II

Solution B: 10 cm of SFRS; 5 cm of simple shotcrete; A500 nails with A_{inf}=3.125 m^2; L=4.00 m ; ϕ 5 mm.

ZG3	W3 a W4	F3 a F4	30-50	30-50	IV a III

Solution C: 20 cm of SFRS; 5 cm of simple shotcrete; A500 nails with A_{inf}=2.0m^2, L=6.00 m and ϕ25 mm; radial drains with ϕ50 mm and L=4.0 m.

Although solution D (ZG4) existed in design, there was no record of areas with such characteristics.

The main results of the tests performed in shotcrete specimens, both simple and reinforced, can be observed in Table 4.

Table 4 – Main characteristics of simple and reinforced shotcrete

BP1 (simple)	
Uniaxial compressive strength	44.5 MPa
BP2 (SFRS)	
Uniaxial compressive strength	47.9 MPa
Energy absorption	1127 J
Dramix fibers dosage	30 kg/m^3

Conditioning Zones

During the excavation phase, three independent areas with poor rock mass quality associated to possible stability issues were detected. These zones were analysed in detail in this work in order to understand if design changes were needed.

The main aspects to investigate are: discontinuities and their orientations, water presence, rock mass permeability and the monitoring results.

The three problematic zones are identified in Fig. 8, and they are descripted below.

PK 1+125 a 1+180 (zone 1)

This zone has a fault crossing the left side of the excavation face, and also a vertical set of discontinuities, which decreases the quality of the rock mass and can cause the instability of the section. Fig. 5 shows some section cartographies in this area and Table 5 presents some rock mass characteristics.

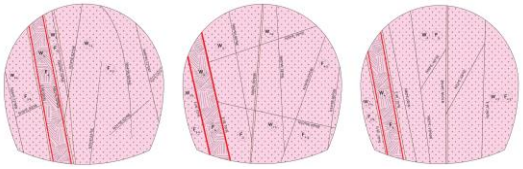

Fig. 5 – Cartographies between 1+125 & 1+180 (ACE, 2010)

Table 5 - Characteristics of zone 1

RMR	**39-42** **Fair to weak**
Subterraneous water conditions	12-14 Between dry and humid
Discontinuities direction	-12 very unfavourable
Tipe of Support predict	C

PK 1+180 a 1+220 (zone 2)

This zone comes right after the previous one and it is very similar to it, although the fault thickens and then it splits into two smaller ones. The characteristics of the rock mass are equal to the ones presented in Table 5, and Fig. 6 shows examples of cartographies sections in this zone.

Unlike zone 1, this zone presented some abnormal convergence results, i.e., even though the displacements were small, they were still increasing (at a small rate) with the excavation face at 1 km away.

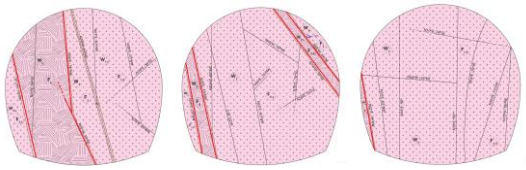

Fig. 6 – Cartographies between 1+180 & 1+220 (ACE, 2010)

PK 2+035 a 2+075 (zone 3)

This zone crosses a fault that shows from the right to the left side of the tunnel cross section (Fig. 5). It has a quartz vein, represented in yellow in Fig. 5, and higher water presence than the other zones observed, as it can be seen in Table 6.

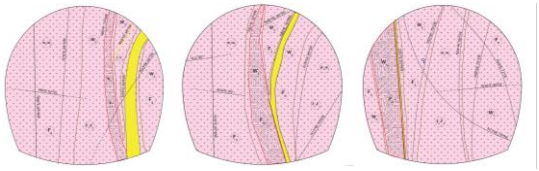

Fig. 7 – Cartographies between 2+035 & 2+075 (ACE, 2010)

Table 6 – Characteristics of zone 3

RMR	**36-42** **Fair to weak**
Subterraneous water conditions	7-12 Between humid and saturated
Discontinuities direction	-12 very unfavourable
Type of Support predict	C

5 Stress-Strain Numerical Analysis

In order to understand the stability issues related to the tunnel, it was performed a numerical analysis in Plaxis 3D, aiming to study the relation between the progress of the excavation face and the resulting displacements.

In the end, it was expected to conclude the allowable maximum lag between the analysed section and the excavation face, without referring any support, and ultimately to predict the best design solution to guarantee stability, considering safety and economic matters.

Table 7 identifies the three most critical cross sections of the three zones under evaluation.

Table 7 – Selected cross sections for analysis

Zone	**1**	**2**	**3**
Cross section	PK 1+151.5 to PK 1+157.0	PK 1+182.0 to PK 1+188.0	PK 2+056.0 to PK 2+060.5

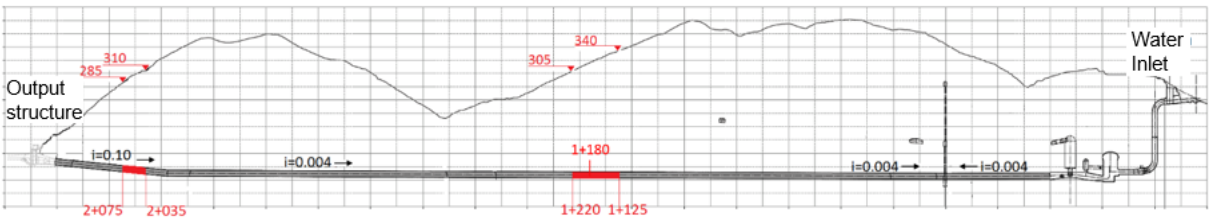

Fig. 8 - Tunnel profile with identification of the 3 critical zones, their mileage and depth (ACE, 2010)

MODEL

The model geometry was defined based on the cross section diameter (D) is 11.3 m, with 5Dx5D square model with horizontal and vertical displacements at the bottom prevented and horizontal displacements at the lateral boundaries also restrained. In order to generate the tensions measured by STT tests, loads were applied in the model to simulate the tension state (Table 8).

Table 8 - In situ stresses according with STT tests

	Section 1	Section 2	Section 3
σ_1 (MPa)	8.1	7.8	5.4
σ_3 (MPa)	4.9	4.7	3.2

The materials were defined according with the fracturing and weathering degrees identified in the cartographies, which are also used to identify the joints. A M-C elastic perfectly plastic model was adopted. The M-C strength parameters were defined by using H-B approximation (Hoek *et al.*, 2002), and the Young modulus was determined by Hoek and Diedrichs (2006) relation. Fig. 9 shows the three different models with material identification, in which, the material separation lines were extended up to the domain limits. Table 9 presents the material characteristics considered in Plaxis.

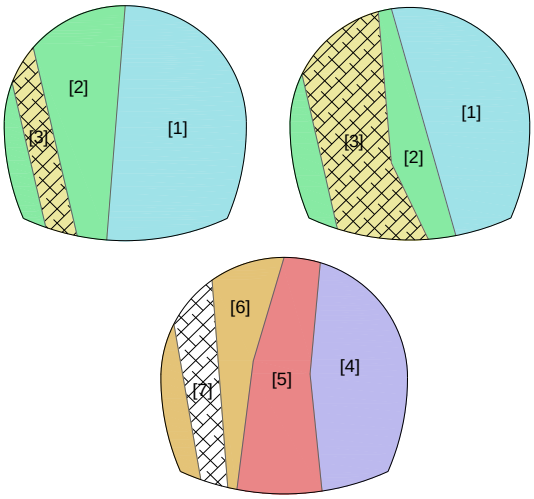

Fig. 9 – Three cross sections geometry with material identification

Table 9 – Mechanical parameters of each section

	MATERIAIS	GSI	E_i (GPa)	E_m (GPa)	υ	ϕ' (º)	c' (kPa)
S1/S2	**[1]** W2-3	43	44.7	26.0	0.23	32.5	370.4
	[2] W3	40		21.2		30.6	339.3
	[3] W4	30		10.8		24.1	244.0
S3	**[4]** W2	43	41.5	24.4		35.9	352.2
	[5] W2-3	40		19.9		31.7	295.5
	[6] W3	37		16.2		26.5	234.6
	[7] W4	30		10.1		22.2	184.6

In addition to materials, it is also necessary to define plate elements, i.e., components with flexural strength to simulate SFRS elements, concrete elements and also a mixed solution that included both SFRS and reinforced concrete elements, as shown in Table 10.

Table 10 – Plates characteristics

Plate	e (m)	EA (kN.m^{-1})	EI (kN.m^2.m^{-1})	υ	W (kN.m^{-2})
Shotcrete	0.2	2.8x10^6	9.33 x10^3	0.23	4.78
	0.3	4.2 x10^6	31.5 x10^3		7.17
	0.4	5.6 x10^6	74.7 x10^3		9.56
Concrete	0.5	11.9 x10^6	247.9 x10^3		11.80
Mixed	0.7	14.7 x10^6	431.6 x10^3		16.59

Finally, to simulate the joints displacement it was necessary to assume the material limits as interfaces, reduced by a strength factor of 75% of the finest granite material in each model. These interfaces allows relative displacement, by taking a virtual thickness of 0.1 m.

Due to memory constraints of Plaxis 3D software, the mesh had to be defined as coarse with a single refinement in the area around the tunnel section. This allowed to replicate the model at each 5 m (single excavation span) up to a 70 m length.

This type of simulation has associated basic errors. While assuming the extension of one single section, the longitudinal heterogeneity is being ignored. This means that the results are conservative, as it is assumed that the less stable cross section is extended by the 70 m.

COMPUTATION PHASE

To understand the rock mass response due to excavation, five points were selected, as shown in Fig. 10, where point A is located at the crown and point B is over the fault, and then measured the convergences over 6 cords, as done in the construction area.

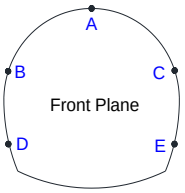

Fig. 10 – Analysed points identification

To simulate the tunnel excavation, each calculation phase was associated with a 5 m advance, in three different situations:

- phased construction with no support;
- phased construction with fiber reinforced shotcrete applied 30 m ahead of the excavation front;
- phased construction with reinforced concrete applied 30 m ahead of the excavation front.

RESULTS ANALYSIS

After running all the models through the 70 m long excavation, it was possible to draw some conclusions. The major displacements occur in the longer cords, i.e., A-D, A-E, D-E, and they all stabilize after 60 m of excavation.

It was only possible to analyse the effect of excavation after passing the analysed cross section. This decision had to be taken due to software memory issues. Displacements taken before the excavation hits the cross section have low values and will not be included in this analysis. It is notorious the effect of the linings in all three cross sections. It was also observed that, when the reinforced concrete was considered, the displacement curve immediately stabilized, due to its high strength and stiffness.

Fig. 11 and Fig. 12 show some of the results at the last calculation phase: Mohr-Coulomb plastic points, principal stress directions and vertical stress. Through the first three images, it is possible to conclude that majority of plastic points are around the tunnel section and the fault area, since these are the areas with larger displacements and stress reliefThe second set of images represents the displacement field with arrows hundred times amplified. It is notorious the movement asymmetry, due to different material characteristics and discontinuity presence. Finally, the last set of images represents the vertical stress, in which it is possible to verify the stress relief surrounding the tunnel. Since cross section 1 and 2 are very close to each other, their depths are similar, resulting in stress values with similar order of magnitude. It is also possible to observe the discontinuities effect, in modifying the stress state, properly simulated as interfaces.

Fig. 10 shows the displacement resultant in the critical points in each cross section. It is possible to observe the displacement stabilization in all the shown cases.

Fig. 11 (cross section 3 – displacement field) and Fig. 13 prove that the convergence measured in Fig. 13 was all due to the left side bench poor material [6], i.e., both convergence value in cord B-C and point B displacement norm have the same value.

ELASTIC STRENGTH VALIDATION OF SUPPORTS

With this numerical analysis it was possible to conclude that if we only consider the stress-strain effect of excavation all the displacements end up to stabilize, meaning that there is no need to introduce structural support in this work. But since this is a hydraulic tunnel, there is still a need to smooth the surface and prevent it from deterioration.

So, it was made a brief elastic validation of the fibber reinforced shotcrete, when it is applied at 30 m distance from the excavation face.

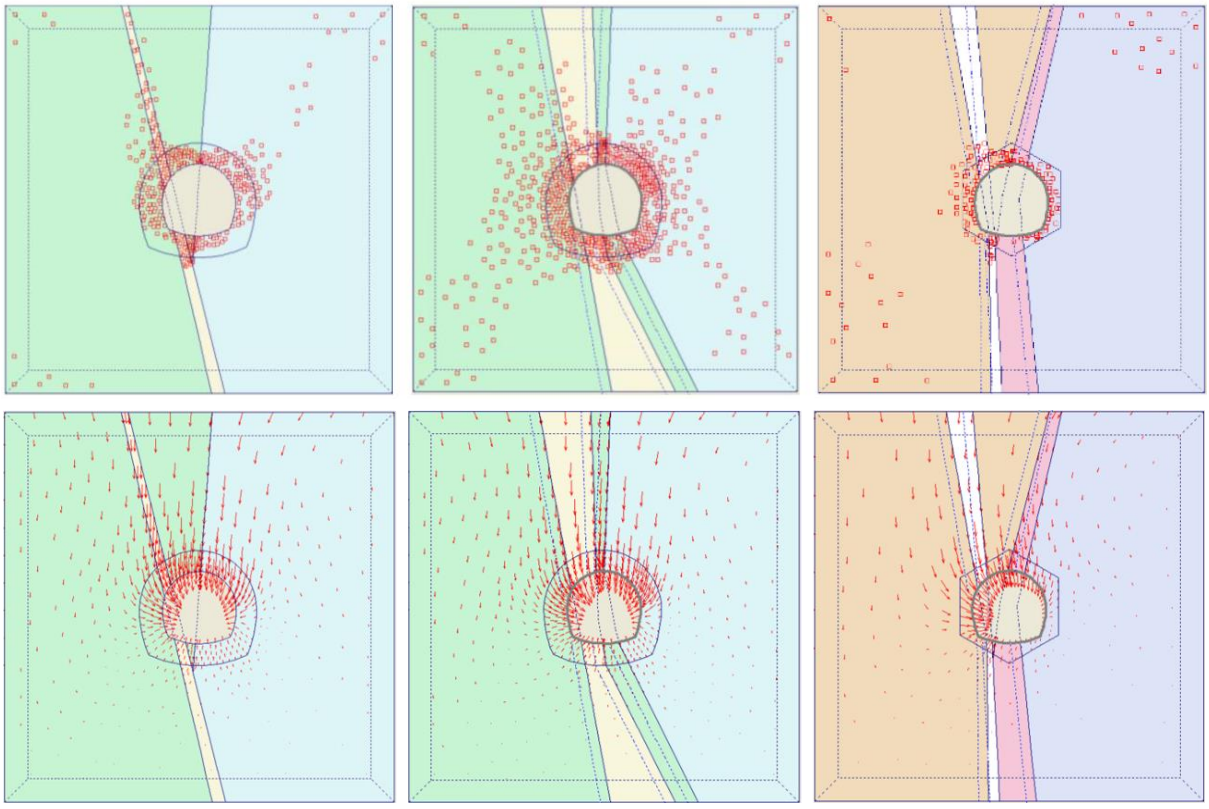

Fig. 11 – Mohr Coulomb Plastic Points and displacement field at the end of the calculation phase

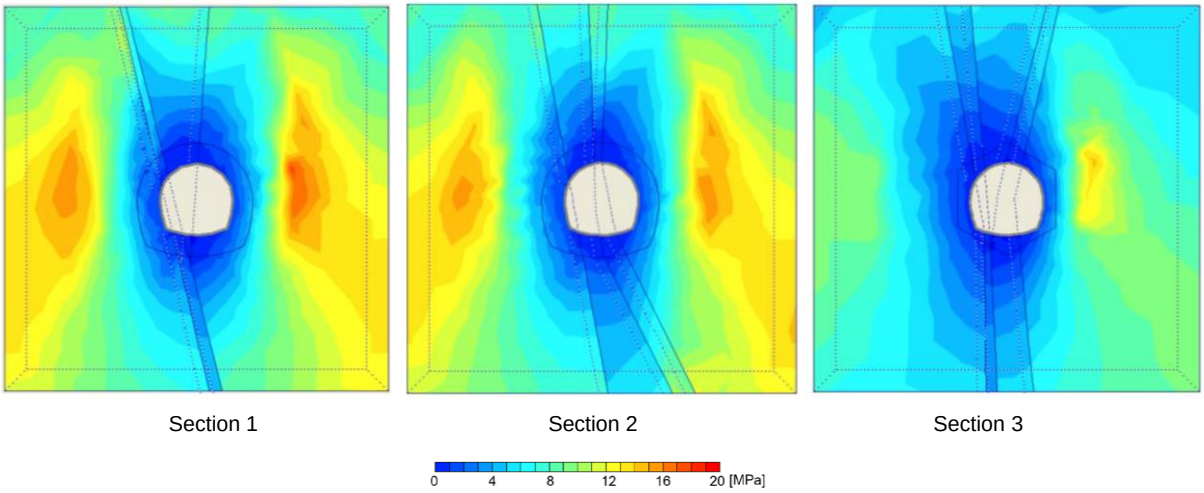

Fig. 12 – Vertical stress of the 3 sections at the end of the calculation phase.

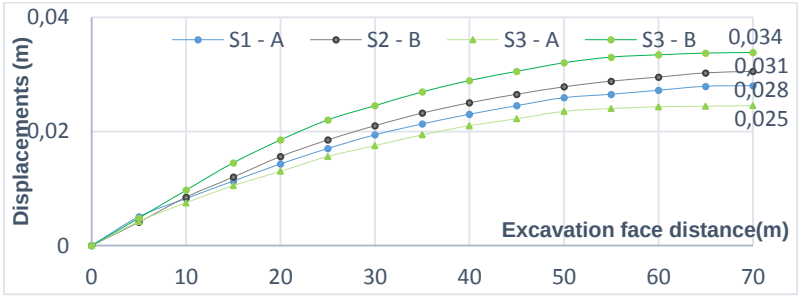

Fig. 13 - Displacements resultant of the most critical points of three different cross sections

Table 11 – Elastic validation of the 3 different linings

	M (kN.m/m)	N (kN/m)	$f_{adm} \geq \frac{N}{e} \pm \frac{M}{w}$ (MPa)	
S1	-5.25	-2228.8	$f_{adm} >$ -11.9	✔
S2	-6.3	-1500.0	$f_{adm} >$ -8.4	✔
	3.9	- 500.0	$f_{adm} >$ -3.1	✔
S3	´-1.66	-1067.0	$f_{adm} >$ -5.6	✔
	5.65	-1461.5	$f_{adm} >$ -8.2	✔
	4.09	-681.7	$f_{adm} >$ -4.0	✔

Since all the linings are elastically verified, the 20 cm fibber reinforced shotcrete solution can be accepted as a final support. Even though nails were not considered in this analysis, it is highly recommended to insert them in a spaced mesh in order to prevent blocks fall.

6 NUMERICAL ANALYSIS OF SEEPAGE

This chapter is intended to study the structural response of the previous design solutions, taking into account the seepage forces.

As observed in Table 5, cross section 1 and 2 are approximately dry, and because of this, seepage forces were not introduced in their analysis.

Cross section 3, on the other hand, is categorized as “saturated to dry” by RMR index (Bienawski, 1989), which also dictates that associated to this category can come a surface water flow of 17.5x10^{-4}m^3/min/m.

Knowing the tunnel diameter (11.3 m) and the flow equation:

$$Q = k.i.D.\pi$$

where Q is the inflow, D the diameter and i the water gradient, and assuming that the fault permeability (k_{fault}) is ten times the rock mass permeability (k_{rm}), it was possible to iterate accurate values to the model parameters (Table 12) in order to obtain the given flow.

Table 12 - Permeability values for numerical modeling

AREA	k_{rm} (m/s)	k_{fault} (m/s)
PERMEABILITY	6.32 x 10^{-8}	10^{-6}

The numerical analysis of cross section 3 included three studies:

i. no support;
ii. 0.20 m of reinforced shotcrete + 0.05 m of plain shotcrete;
iii. 0.50 m of reinforced concrete + 0.20 m of reinforced shotcrete + 0.05 m of plain shotcrete.

By means of performed phreatic level measurements and knowing the proximity of this zone to the river, it was assumed a 80 m water column at the cross section tunnel axis. After

introducing boundary conditions in order to generate the appropriate model water pressures, it was imposed a zero pressure condition inside the tunnel section, since this tunnel is in direct contact with the atmosphere.

The first model, with no support, proved of the need for some kind of lining. That is, as it can be observed in Fig. 14, water flow velocity is extremely high, which results in high water gradients (1 to 7). This type of values, higher than 5, are associated with fines entering of the filling of the fault zones.

Fig. 14 shows the water velocities diagrams, with the maximum value indicated for the two other solutions, and Fig. 16 shows the pore pressure distribution. The permeability assumed for the concrete and shotcrete was k_c=10^{-9} m/s.

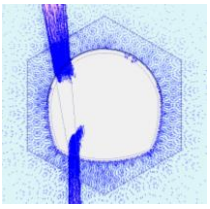

Fig. 14 – Water flow velocity vectors with solution (i)

It is possible to verify that in both cases the velocity abruptly increases in the fault area. This fact is justified by the lowering of pore pressures due to higher permeability (Fig. 16).

In solution (iii), Fig. 15 shows a reversal on the velocity direction, towards the upper domain limit. This occurs because, since the lining is thicker in solution (iii), the pressure gradient is higher, which results in higher values of pressure on the tunnel surroundings. As the water preferred path is in direction to the lowest pressure, it is now possible to understand why this happens.

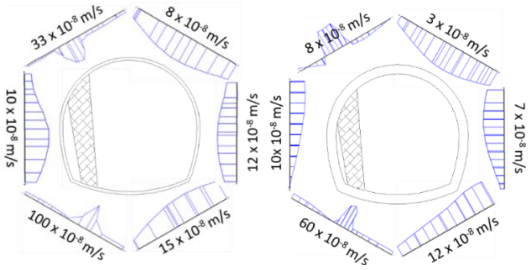

Fig. 15 – Water flows velocities diagrams for solution (ii) and (iii)

STRESS-STRAIN ANALYSIS WITH SEEPAGE FORCES

The 2D seepage analysis allowed estimating the pore pressures that would affect the tunnel support in each different solution. So it was necessary to introduce these forces and try to validate the previous conclusions. In order to accomplish that, the pore pressures were measured in a hexagon circumscribed to the tunnel cross section, and then introduced in Plaxis 3D tunnel stress-strain model (Fig. 17). After introducing these forces, the lining stresses were higher and didn't verify the elastic criterion (Table 13).

Even though the 25 cm of SFRS would probably have a failure validation, it was studied three other solutions, in which all the pore pressure equivalent loads were properly modified, the (iii) one and two new ones:

i. 0,35 m of reinforced shotcrete + 0,05 m of simples shotcrete;
ii. 0,45 m of reinforced shotcrete + 0,05 m of simple shotcrete;

The results are shown in Table 14.

Table 13 – Elastic validation of solution (ii)

	M (kN.m/m)	N (kN/m)	$f_{adm} \geq \frac{N}{e} \pm \frac{M}{w}$ (MPa)	
(ii)	-9.4	-2676	$f_{adm} <$ -14.8	⊘
	11.2	- 3181	$f_{adm} <$ -17.8	⊘

Table 14 - Elastic validation of the new solutions

	M (kN.m/m)	N (kN/m)	$f_{adm} \geq \frac{N}{e} \pm \frac{M}{w}$ (MPa)	
(iv)	-22.0	-3300	$f_{adm} >$ -12.5	✔
	30.1	-3500	$f_{adm} <$ -15.9	⊘
(v)	-22,4	-2157	$f_{adm} >$ -6.2	✔
	64.2	-2250	$f_{adm} >$ -8.0	✔
(iii)	-94.5	-4099	$f_{adm} >$ -6.5	✔
	210.6	-4257	$f_{adm} >$ -7.9	✔

The above table shows that only the solution (iii) and (v) present elastic validation. Since reinforced concrete is a more complex and expensive solution, by this analysis, the ideal support would be 40 cm of SFRS plus 5 cm of simple shotcrete.

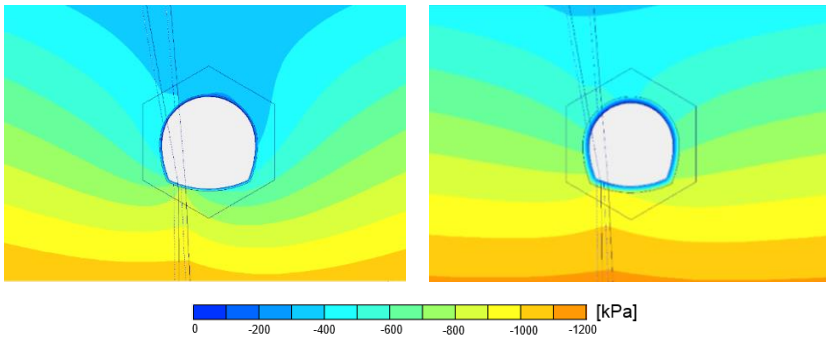

Fig. 16 – Pore pressure distribution for solution (ii) and (ii

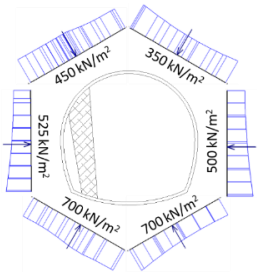

Fig. 17 - Solution (ii) pore pressures.

7 Conclusions and Further Investigation

Hoek-Brown criterion takes into account the rock mass heterogeneity and anisotropy, which make it a realistic approximation of the material response.

Shotcrete solutions are not only more economic, as they present as good strength and isolation performance as the reinforced concrete ones.

Three-dimensional numerical analysis allowed the study of the tunnel response to the advance of the excavation face. This simulation certified that two of the study cross sections did not need any structural support, but with the presence of seepage forces, the third one would need a thicker shotcrete/concrete lining. Even without the need of support, a shotcrete lining is always recommended in a hydraulic tunnel in order to smooth the surface and to prevent it from deterioration and to comply with seepage effects.

Once the granitic rock mass has such high quality, there was no need to consider nails in the simulation model. But they still have an important role in preventing rocks fall.

The major constraints of this work were:

- the fact that there is no way to know in which discontinuity the failure will happen, since the rock mass is being studied as a homogenous material;
- There were not enough boreholes and tests to correctly characterise the critical areas;
- The 3D software (Plaxis 3D Tunnel 1.2) used is quite simplistic and had some memory limitations.

Further Investigation

It would be interesting to use a software that allowed a complete 3D simulation, with the possibility of changing the full longitudinal profile in order to build a more accurate model. And also develop a way of imposing *in situ* stresses, because in rock masses this are not so easy to simulate with equivalent loads, since the stresses distribution is not only gravity induced.

It is also suggested to make a similar analysis but using the Jointed Rock model, in which the presence of joint sets are taking into account.

Other useful study, would be the development of monitoring instrumentation that allowed a fully perception of cross sections displacements, even before the excavation face reached the point.

Lastly, there were some constraints in analytically design the SFRS, due to the lack of information about this material. Hence, the fully study and comprehension of SFRS, would be able to qualify works and designs.

8 References

ACE (2010). Reforço de Potência da Barragem de Salamonde II, Empreitada Geral de Construção, Volume VII – Estudo de Caracterização Geológica e Geotécnica.

Álvarez, D.L. (2012). Limitations of the Ground Reaction Curve Concept for Shallow Tunnels Under Anisotropic In-situ Stress Conditions. MSc Thesis. KTH Architecture and the Built Environment, Stockholm, Sweden.

Aydan, Ö., Akagi, T., Kawamoto, T. (1993). *The squeezing potencial of rocks around tunnels; theory and prediction*. Rock mech. Rock Engng., 26, 2, pp. 137-163.

Barton, N., Lien, R., Lunde, J. (1974). *Engineering Classification of Rock Masses for the Design of Tunnel Support*. Rock Mechanics 6, pp.189-236.

Bieniawski, Z.T. (1989). *Engineering Rock Mass Classifications*. Wiley, New York.

Hoek, E. (1994). "Strength of Rock and Rock Masses", ISRM News Journal, volume 2, n.2 pp 4-16.

Hoek, E. Carranza-Torres, C., Corkum, B. (2002). *Hoek-Brown Failure Criterion* – 2002 Edition. NARMS-TAC Conference, Toronto.

Hoek, E.,Diederichs, M.S. (2006). *Empirical estimation of rock mass modulus*. International Journal of Rock Mechanics and Mining Sciences, volume 43, pp. 203–215.

Hudson, J.A., Harrison, J.P. (1997). *Engineering rock mechanics*. Pergamon, Oxford.

Kim, K., Franklin, J.A. (1987). *Suggested Methods for Rock Stress Determination*. International Journal of Rock Mechanics and Mining Sciences, volume 24, pp. 53-73.

Lamas, L., Figueiredo, B. (2009). *Reforço de Potência de Salamonde – Ensaios com defórmetro tridimensional para determinação do estado de tensão*. I&D Barragens de Betão, Relatório 403/2009 – NFOS, LNEC, Lisboa.

Vandewalle, M. (2005). *Tunnelling is an Art*. NV Bekaert SA, Zwevegem, Belgium.

Vallejo, L.I.G., Ferrer, M. (2011). *Geological Engineering*. Taylor & Francis Group, London.